Modulation of magmatic processes by CO_2 flushing

Caricchi, Luca; Sheldrake, Thomas Edward; Blundy, Jon

How to cite

CARICCHI, Luca, SHELDRAKE, Thomas Edward, BLUNDY, Jon. Modulation of magmatic processes by CO_2 flushing. In: Earth and Planetary Science Letters, 2018, vol. 491, p. 160–171. doi: 10.1016/j.epsl.2018.03.042

This publication URL: https://archive-ouverte.unige.ch/unige:103444
Publication DOI: 10.1016/j.epsl.2018.03.042

Modulation of magmatic processes by CO_2 flushing

Luca Caricchi[1], Tom E. Sheldrake[1], Jon Blundy[2]

1) Department of Earth Sciences, University of Geneva, Rue des Maraîchers 13, 1205, Geneva, Switzerland

2) School of Earth Sciences, University of Bristol, Wills Memorial Building, BS8 1RJ, Bristol, UK

Abstract

Magmatic systems are the engines driving volcanic eruptions and the source of fluids responsible for the formation of porphyry-type ore deposits. Sudden variations of pressure, temperature and volume in magmatic systems can produce unrest, which may culminate in a volcanic eruption and/or the abrupt release of ore-forming fluids. Such variations of the conditions within magmatic systems are commonly ascribed to the injection of new magma from depth. However, as magmas fractionating at depth or rising to the upper crust release CO_2-rich fluids, the interaction between carbonic fluids and H_2O-rich magmas stored in the upper crust (CO_2 flushing), must also be a common process affecting the evolution of subvolcanic magma reservoirs. Here, we investigate the effect of gas injection on the stability and chemical evolution of magmatic systems.

We calculate the chemical and physical evolution of magmas subjected to CO_2-flushing using rhyolite-MELTS. We compare the calculations with a set of melt inclusion data for Mount St. Helens, Merapi, Etna, and Stromboli volcanoes. We provide an approach that can be used to distinguish between melt inclusions trapped during CO_2 flushing, magma ascent and decompression, or those affected by post-entrapment H_2O-loss. Our results show that CO_2 flushing is a widespread process in both felsic and mafic magmatic systems. Depending upon initial magma crystallinity and duration of CO_2 input, flushing can either lead to volcanic eruption or fluid

release. We suggest that CO_2 flushing is a fundamental process modulating the behaviour and chemical evolution of crustal magmatic systems.

1. Introduction

Magmatic fluids are mainly composed of H_2O and CO_2, the latter being significantly less soluble in silicate melts (Ghiorso and Gualda, 2015; Newman and Lowenstern, 2002). Crystallisation of silicate magma at depth and/or its ascent through the crust leads to preferential release of CO_2-rich fluids (Blundy et al., 2010; Newman and Lowenstern, 2002; Papale et al., 2006), such that magmas stored in the upper crust contain 40-60 times more H_2O than CO_2 (GEOROC database; Fig. 1a; Barsanti et al., 2009). Thus, magmas stored at shallow depths are, in effect, high temperature chemical reactors exposed to flushing of hot CO_2-rich fluids released from deeper in the magmatic system (Barsanti et al., 2009; Blundy et al., 2010; Evans et al., 2016; Metrich et al., 2004; Moretti et al., 2013; Yoshimura and Nakamura, 2011; 2010). Similar interactions between CO_2-rich fluids and magmas can also occur in carbonate-hosted magmatic systems (Blythe et al., 2015; Cross et al., 2013; Di Rocco et al., 2012; Iacono Marziano et al., 2007; Jolis et al., 2013; Mason et al., 2017; Preece et al., 2014).

An increase in the partial pressure of CO_2 in the fluid phase in equilibrium with a magma, produced either by CO_2 flushing or by interaction with carbonate, leads to the dissolution of modest amounts of CO_2 in the melt and exsolution of several wt.% of H_2O (Ghiorso and Gualda, 2015; Newman and Lowenstern, 2002; Yoshimura and Nakamura, 2011; Fig. 1a, b). The effects are a net increase of magma volume (i.e. excess fluid volume fraction), progressive magma crystallisation due to reduced weight fraction of dissolved H_2O (Fig. 1a,b; Blundy and Cashman, 2008; Blundy et

al., 2010; Riker et al., 2015), and changes in crystallising assemblage and mineral chemistry (Riker et al., 2015).

Previous studies have applied Rhyolite-MELTS (Gualda et al., 2012) to quantify the effect of crystallisation and excess volatile exsolution on the evolution of the physical properties of magma and fluid overpressure (Tramontano et al., 2017; Fowler and Spera, 2008). Here, we use Rhyolite-MELTS to simulate interaction between CO_2-rich fluids and magmas stored in the upper crust and quantify the impact of this process on the chemical and physical evolution of the system. We also simulate simple, adiabatic decompression of volatile-bearing magmas to compare the effects of these two contrasted processes on the chemical evolution of the residual melt (i.e. melt in equilibrium with fluid phase and crystals). The results of our calculations allow us to explore melt inclusion data collected in systems for which extensive datasets exist (Mt. St. Helens, Merapi, Etna and Stromboli; GEOROC and Blundy et al., 2010; Metrich et al., 2010; Preece et al., 2014). We propose a new approach that can be applied to melt inclusions datasets to distinguish between magma-ascent, interaction with CO_2-rich fluids or post-entrapment H_2O loss. The application of this method to felsic and mafic magmatic systems (GEOROC and Blundy et al., 2010; Metrich et al., 2010; Preece et al., 2014) show that melt inclusion data invariably record interaction between magma and CO_2-rich fluids. Consequently, we focus on the impact of CO_2 flushing on the evolution of the chemical and physical properties of upper crustal magma reservoirs, and discuss the influence of CO_2 flushing on the ability of a magma reservoir to erupt magma and/or release magmatic volatiles.

2. Methods

2.1 Rhyolite-MELTS

We performed calculations using the thermodynamic software Rhyolite-MELTS (version 1.1.0; Ghiorso and Gualda, 2015; Gualda et al., 2012) to simulate the effects of CO_2 flushing and adiabatic ascent on the chemical and physical evolution of volatile-bearing magma. The chemical interaction between pure, hot CO_2 and magma is performed considering no subsequent heat loss from the system. CO_2 is injected at the liquidus temperature of the magma. In the calculations we consider either an initially H_2O-saturated (CO_2-free) rhyolitic magma (composition equivalent to the average melt inclusion composition of the early phase of the Bishop Tuff eruption: Gualda et al., 2012; Ghiorso and Gualda, 2015) or a H_2O-bearing basalt (Etna; melt inclusion composition MI 33 of Metrich et al., 2004; 3 wt. % H_2O; Tables 1, 2) at their respective liquidus temperatures. Rhyolite-MELTS was chosen as it performs all thermodynamic calculations with the latest available solubility data for magmas of a wide variety of compositions (Ghiorso and Gualda, 2015). Simulations were carried out at fixed confining pressures of 100, 200 and 300 MPa and constant oxygen fugacity (fO_2). Simulations for Bishop Tuff and Etna compositions were completed with fO_2 = NNO (Tables 1, 2). To check for the effect of redox state additional simulations for the Etna composition were performed at fO_2 = QFM (Table 1S). We simulate isenthalpic assimilation of a fluid phase composed of pure CO_2. CO_2 is added in steps of 0.01 grams up to a total of 10 grams of CO_2 for 100 grams of magma. Thermodynamic equilibrium is achieved at each step of the calculations between melt, injected fluid and crystals (i.e. we consider crystallisation at equilibrium).

A second set of simulations was performed to simulate adiabatic ascent of volatile-bearing magma: 1) isentropic ascent with the same compositions as those used for the CO_2 flushing simulations, but with the magma initially containing some CO_2 (Tables

1, 2); 2) ascent of magma initially containing excess fluids (Tables 1, 2). In both cases, the starting composition was equilibrated at fO_2 = NNO buffer, but left free to vary during magma ascent and degassing.

In all simulations we trace the evolution of magma volume, temperature, crystallinity, and residual melt chemistry (Figs. 2-5) to provide insights into how CO_2 flushing and adiabatic ascent of magmas influence respectively the chemical variability and volatile content of melt inclusions. We consider closed-system (no release of excess fluids) and thermodynamic equilibrium in our simulations. The release of the excess volatile phase, if equilibrium between fluid and magma is maintained, does not affect the chemical evolution of the system. However, as discussed more extensively in Section 4.2, the release of a portion of the excess fluids can affect the total volume increase of the system and magma compressibility, thus influencing the overpressure produced. Whilst, closed-system assumption might be more conceivable for large silicic systems in comparison to more dynamic basaltic open-conduit systems, we focus on closed system conditions to understand the effects of CO_2-flushing on magmatic systems of varying chemistry.

2.2. Melt inclusions calculations

We calculated pressure of entrapment, and composition (xH_2O) of the excess fluid phase for melt inclusions (MI) assuming entrapment at fluid-saturated conditions. We do not consider the individual composition of each melt inclusions when computing entrapment pressure and the composition of the excess fluid phase, but consider instead generic solubility models applicable to felsic and mafic compositions from Ghiorso and Gualda (2015). Calculations for Mount. St. Helens and Merapi MIs were performed with the solubility model provided for the Bishop Tuff in Ghiorso and

Gualda, (2015). For Etna and Stromboli MIs, we considered the H_2O-CO_2 solubility model provided for MORB in Ghiorso and Gualda (2015). We calculate the entrapment pressure and the composition of the excess fluid phase by determining the isobar and fluid isopleth passing through the H_2O and CO_2 content of each MI. The resulting entrapment pressure and composition of the excess fluid phase are combined with their K_2O content, a proxy for magma crystallisation, to identify the processes responsible for MI entrapment and chemical composition. Note that K_2O can be substituted by any other element that is incompatible during crystallisation.

To test the reliability of our generic solubility approach, we calculated the entrapment pressure for several pairs of melt inclusions (a couple from Merapi and Mt. St. Helens, and another from Stromboli-Etna) considering explicitly their compositions and using MagmaSat (Ghiorso and Gualda, 2015) to calculate pressure and fluid chemistry. The comparison between the calculations performed with our approach and MagmaSat, shows that the uncertainty is never larger than ±25 MPa and about 0.05 in xH_2O (Figs. 6, 7).

3. Results

3.1. CO_2 - magma interaction

The progressive addition of CO_2 to H_2O-saturated magma at constant confining pressure leads to progressive dissolution of CO_2 and concomitant exsolution of H_2O (Fig. 1) leading to an increase in the mass of excess fluid phase in equilibrium with the magma (Figs. 1, 2a, 3a). The impact of CO_2 flushing on melt fraction and temperature differs between felsic and mafic magmatic systems (Fig. 2, 3). For felsic magma, the molar fraction of H_2O in the excess fluid phase (xH_2O_{fluid}) decreases as a consequence of the increasing amount of CO_2 added to the system and the minor

amount dissolved in the residual melt phase (Fig. 2). The decrease of H_2O concentration in the residual melt phase drives magma crystallisation due to liquidus temperature increase (Fig. 2b; Riker et al., 2015). As the calculations were performed at isenthalpic conditions (no exchange of heat with the exterior), the release of latent heat of crystallisation during CO_2 flushing results in an increase of temperature, which is more pronounced with decreasing confining pressure (Fig. 2c). In contrast, in mafic magma CO_2 flushing leads to progressive dissolution of CO_2, but exsolution of H_2O is delayed until the system reaches fluid saturation (Fig. 3). The lower amount of H_2O initially dissolved in the mafic magma results in a smaller drop of the residual melt fraction during progressive CO_2 addition (Fig. 3b). In turn, this leads to the progressive drop of temperature, as the latent heat of crystallisation is insufficient to compensate for the heat required for excess fluid vaporisation (Fig. 3c).

Residual melt chemistry also changes with CO_2 flushing because of progressive magma crystallisation. We plot the results of the thermodynamic calculations considering H_2O, CO_2 and K_2O concentration in the residual melt combined with the evolution of the molar fraction of xH_2O in the excess volatile phase (Fig. 4). We have selected these parameters because their evolution during CO_2-flushing, magma ascent (Blundy and Cashman, 2008) and post-entrapment H_2O loss (Gaetani et al., 2012) is different. This provides a chance to distinguish between these processes simply from analysis of melt inclusion data. CO_2 flushing at constant confining pressure produces a decrease of H_2O in the residual melt accompanied by an increase of CO_2 and K_2O (Fig. 4). The variations occur together with a progressive decrease of xH_2O in the excess fluid phase (Fig. 4b). Magmas initially containing lower H_2O (e.g. Etna with respect to Bishop Tuff), exposed to CO_2-flushing, experience less crystallisation than magmas containing more H_2O for comparable drops in xH_2O_{fluid} (Fig. 4b, d). This

manifests graphically as a steeper drop of xH_2O_{fluid} with respect to the decrease of K_2O_{min}/K_2O in the residual melt (Fig. 4b, d; where K_2O_{min} is the lowest content of K_2O in the set of melt inclusions of interest, i.e. the K_2O of the less chemically evolved MI).

Results of calculations performed for the Etna composition at fO_2 = QFM buffer, are almost identical to those performed at NNO (Tables 1, 2; Figs. 3, S1).

3.2. Variation of residual melt chemistry during magma ascent

We calculate the evolution of residual melt chemistry during magma ascent to identify differences to the variations produced by CO_2-flushing. Results, presented in H_2O-CO_2 and K_2O_{min}/K_2O – xH_2O_{fluid} space (Fig. 5), show that the increase of K_2O content of the residual melt phase occurs at relatively low pressure only after significant amounts of H_2O have been lost to the excess volatile phase (Fig. 5). This modest K_2O increase is associated with the limited crystallisation occurring at intermediate to high pressure (500-200 MPa) during magma ascent (Fig. 5a). Upon decompression xH_2O_{fluid} increases while K_2O_{min}/K_2O of the residual melt only starts to increase at the pressure at which significant H_2O degassing occurs (Fig. 5b, d; Papale, 2005).

We tested also the effect of excess fluid on the evolution of residual melt chemistry upon magma ascent using the Etna composition and considering an exsolved fluid phase already present at depth (Fig. 5d; Table 1). The initial presence of excess CO_2-rich fluids promotes magma crystallisation and limits the increase of xH_2O_{fluid} upon ascent (Fig. 5e, f). As identified in previous melt inclusions studies, if sufficient excess fluid is present initially, the volatile content of the ascending magma can follow an isopleth corresponding to the molar ratio of CO_2 and H_2O in the excess fluid phase (Metrich et al., 2004). However, we note that even in the presence of an

excess fluid phase, decompression between 500 and 200 MPa results in a modest amount of crystallisation (Fig. 5e, f). Increasing the mass of excess fluid by a factor of five with respect to the amount reported in Table 1 produced results similar to those reported in Figure 5e and f.

In summary, thermodynamic calculations performed to simulate CO_2-flushing and magma ascent show that the residual melt chemistry changes in very distinctive ways for these two processes. Therefore, the analysis of dissolved volatile content and chemistry of melt inclusions remains a useful tool to probe processes accompanying magma transfer and storage in the crust.

3.3 Melt inclusions

Once any effects of post-entrapment processes are accounted for, MIs can provide information on magmatic processes taking place in crystallising portions of magmatic systems (Metrich et al., 2004; Blundy and Cashman, 2001; Gaetani et al., 2012; Papale, 2005). The relative chemical signals of magmatic and post-entrapment processes can be deconvolved through the combined analysis of MI volatile content and chemistry (inset Fig. 6b). Ascent of fluid-saturated magmas triggers exsolution of volatiles, which are initially dominated by CO_2 (Ghiorso and Gualda, 2015; Newman and Lowenstern, 2002). As ascent continues, the amount of CO_2 dissolved in magma decreases and the proportion of H_2O in the exsolved fluid phase increases (Fig. 5). If ascent is accompanied by crystallisation (Blundy et al., 2010), MIs will record this process with specific CO_2-, H_2O- and K_2O trends (Fig. 5). Post-entrapment hydrogen loss from MIs (Gaetani et al., 2012) leads to a simultaneous decrease in H_2O and increase in CO_2 with respect to chemical trajectories produced by fluid-saturated magma ascent but without variation of MI chemistry (inset Fig. 6a,b). CO_2 flushing

leads consistently to a decrease of dissolved H_2O and the combined increase of CO_2 and incompatible elements such as K_2O (Figs. 2-4, 6).

We consider MI data from four well-studied felsic and mafic volcanic systems (Mount St. Helens, Merapi, Etna and Stromboli; GEOROC; Blundy et al., 2010; Metrich et al., 2010; Preece et al., 2014). In all systems, MIs with the highest K_2O content contain the lowest H_2O (Figs. 6a,c; 7a, c). Whereas ascent-induced crystallisation can be responsible for the high K_2O of MIs with the lowest H_2O and CO_2 content, only CO_2 flushing can produce water-poor and CO_2 and K_2O-rich melt inclusions (Figs. 6a, c; 7a, c). The same conclusion is reached when projecting the data in K_2O_{min}/K_2O – xH_2O_{fluid} space (Figs. 6b, d; 7b, d). MI for Mount St. Helens and Merapi seem dominated by the effects of CO_2 flushing, while a minority can be explained by ascent-induced crystallisation or H_2O-loss (Fig. 6). This interpretation differs from that of Blundy and Cashman (2005). In basaltic systems most of the melt inclusions can be explained by CO_2 flushing or ascent of magma initially saturated in CO_2-rich fluids ($0.25<xH_2O<0.4$; Fig. 7).

3.4. Evolution of physical properties of magma undergoing CO_2 flushing

Melt inclusion data show that CO_2 flushing is an important process to consider for the chemical evolution of magmas in the crust. As CO_2 flushing is accompanied by exsolution of volatiles, increase in magma volume and crystallisation (Fig. 1), the consequent evolution of physical properties determines the potential for CO_2 flushing to trigger volcanic eruptions or the release of fluids from magma reservoirs (Figs. 1-3). The increase of volume associated with the presence of excess fluid is larger at lower confining pressure because of the effect of fluid compressibility (Pitzer and Sterner, 1994; Sterner and Pitzer, 1994; Fig. 8a, b, c). Conversely, as the solubility of

volatiles increases with confining pressure, the amount of H_2O released during CO_2 flushing increases with confining pressure (Fig. 8d, e, f). The residual melt fraction decreases during flushing together with xH_2O_{fluid} (Fig. 8). As the mass of injected CO_2 increases the excess fluids become progressively more carbonic as shown previously by Yoshimura and Nakamura (2011). The rate of volume expansion, H_2O release, and crystallisation are all highest for relatively small amounts of added CO_2, i.e. less than 0.5-1 wt.% (Fig. 8).

An example can be used to elucidate the progressive evolution of magma undergoing CO_2 flushing. A magma with the Bishop Tuff composition and an initial melt fraction of 0.8, progressively flushed with CO_2, will progressively readjust its dissolved and exsolved fluid composition until a total of about 9 wt.% fluid at 100 MPa and 8 wt.% at 300 MPa has been added to the system (grey arrows in Fig. 8). At this point the excess fluid fraction, considering a closed system, will be 0.55 at 100 MPa and 0.3 at 300 MPa. The residual melt fraction will have decreased from 0.8 to 0.2 at 100 MPa and to 0.3 at 300 MPa (Fig. 3). While these calculations are strictly valid only for the Bishop Tuff composition, the general evolution of crystallinity and composition of the excess fluid phase for other magmas will be similar.

4. Discussion

4.1. Interpreting melt inclusions

Most of the MIs from Mt. St. Helens and Merapi can be explained by residual melt evolution resulting from CO_2 flushing, with a subset suggesting trapping during ascent (Fig. 6). In mafic systems such as Etna and Stromboli, the MIs with the highest water content and variable CO_2 describe a trend that can be explained with entrapment during magma ascent in the presence of sufficient excess fluid to, at least

partially, buffer xH_2O in the fluid phase (Fig. 7). Rhyolite-MELTS simulations of the evolution of H_2O- and CO_2-bearing magma during adiabatic ascent to the surface show that there is little or no crystallisation until the pressure drops to less than ~120 MPa (Fig. 5a, b). This is unsurprising given that ascent-induced crystallisation only occurs once significant amounts of H_2O are lost from the residual melt phase, or if significant cooling occurs during ascent (Blundy and Cashman, 2001; Blundy et al., 2010; Papale, 2005). However, the implications for the interpretation of MIs are significant. If no crystallisation occurs, MIs cannot be trapped, which accounts for the paucity or total absence of H_2O-rich MI containing CO_2 over a wide range of concentrations (Fig. 6). For systems such as Etna and Stromboli MI with the highest H_2O and CO_2 content are rare and their dissolved volatile content is likely to represent minimum estimates as no crystallisation can occur at higher pressures, when magma is strongly H_2O-undersaturated (Fig. 7). This implies that melt inclusions data provide only partial information on the ascent path of magmas from the lower crust to the surface. We notice that for Etna and Stromboli, the large amount of melt inclusions containing variable CO_2 and relatively constant H_2O could be also explained by trapping over a variety of pressure during crystallisation. This would also imply that the crystals containing these MIs have been remobilised during the ascent of a magma batch feeding a volcanic eruption.

For Stromboli melt inclusions concentrate along the xH_2O 0.3 isopleth, which could indicate that the concentration of H_2O and CO_2 in the melt (and recorded by the melt inclusions) is controlled by the composition of the excess fluid phase. In an open conduit system such as Stromboli, it is plausible that magma fills the plumbing system over a range of depths and fluids of deeper origins buffer xH_2O of the excess fluid phase.

4.2. CO_2-induced destabilisation of magmatic systems

Both crystallisation and magma ascent lead to the release of carbonic fluids once fluid saturation is achieved. The CO_2-rich fluids can interact with upper crustal magma reservoirs triggering variations in the physical properties of magma. The increase of magma volume associated with CO_2 flushing (Fig. 3,8) can generate overpressure, and potentially destabilise the magmatic system leading to volcanic eruption. However, whether this happens will depend on the crystal content of the magma, which reduces magma mobility and increases with progressive addition of CO_2. If magma reaches its rheological locking point (Marsh, 1981), the chance that the CO_2-flushed magma will feed volcanic eruptions drops rapidly. Thus, in this scenario, CO_2 flushing will promote magma storage and the release of excess fluids without associated magma (Parmigiani et al., 2016). Moreover, with progressive addition of CO_2, magma compressibility increases and the efficiency of CO_2 flushing in generating volumetric expansion and, potentially, overpressure decreases (Fig. 8).

To explore whether CO_2 flushing induces eruption or release of fluids, we calculate the overpressure generated by CO_2 flushing and compare the timescales required to pressurise the reservoir to values compatible with volcanic eruptions to the viscous relaxation timescales of the upper crust (Jellinek and DePaolo, 2003; Rubin, 1995). Pressurisation of a magma reservoir to values sufficient to trigger eruption ($10<\Delta P_{crit}<40$ MPa;) can occur if the increase of magma volume occurs on timescales shorter than the those required for viscous relaxation of the surrounding crust (Jellinek and DePaolo, 2003; Parmigiani et al., 2016). Additionally, the progressive decrease of magma density associated with the increase of excess volatiles will increase buoyancy and contribute to destabilisation of magmatic systems (Caricchi et al., 2014). The

value of ΔP_{crit} is controlled by the overpressure required to propagate a dyke to the surface without freezing (Rubin, 1995; Jellinek and DePaolo, 2003). The value of ΔP_{crit} varies with magma composition and tectonic setting and here we select a range appropriate for felsic magmas.

To explore the pressurisation of a CO_2-flushed magma reservoir we performed calculations for plausible conditions using the results of the Rhyolite-MELTS simulations. We considered a cylindrical, 1 km-thick, 5000 km^3 magma reservoir with the Bishop Tuff composition embedded at depths equivalent to 100 and 300 MPa pressure in a crust with viscosity between 10^{19} and 10^{20} Pa s (Jellinek and DePaolo, 2003). The reservoir is flushed with pure CO_2 at a mass flux between 10^{-7} and 10^{-3} $mol/m^2/s$, consistent with surface observations at volcanoes (Federico et al., 2010; Werner and Brantley, 2003). Fluid transport modelling shows that, regardless of the mechanism of fluid percolation through a magma reservoir, fluid ascent velocity is sufficiently low to enable complete chemical equilibration between fluid and magma (Federico et al., 2010; Werner and Brantley, 2003; Yoshimura and Nakamura, 2011). Thus, once the CO_2-rich fluid front reaches the top of the magmatic system (1 year for a system of 1 km thickness; Yoshimura and Nakamura, 2011), the rate of volume increase of the reservoir is controlled only by the mass flux of injected fluid. We note that the results are valid for the explored range of CO_2-fluxes for reservoirs of different volumes, provided that the reservoir thickness remains at 1 km. For thicker reservoirs, the time required for the fluid to reach the top of the system will increase (Yoshimura and Nakamura, 2011). We calculate the viscous relaxation timescale of the crust as (Jellinek and DePaolo, 2003):

$$\tau = \frac{\eta_{crust}}{E} \qquad (1)$$

where η_{crust} is its viscosity and E its elastic modulus (≈10 GPa). The overpressure (ΔP) resulting from CO_2-magma interaction is calculated as (Tramontano et al., 2017):

$$\Delta P = \frac{dV}{V_{res}} \cdot \frac{1}{\beta} \quad (2)$$

where dV is the volume change, V_{res} is the reservoir volume and β is magma compressibility. dV and β are provided by the Rhyolite-MELTS calculations.

We focus our analysis on the first 0.1 wt.% of CO_2 added where the rate of pressure increase is highest (Fig. 3). Results show that whether CO_2 flushing can trigger an eruption or provoke release of magmatic fluids depends on: the initial melt fraction of the magma; the depth of the reservoir; the critical overpressure required to trigger eruption; and the timescale over which CO_2 is added. CO_2 flushing of magma reservoirs containing eruptible magma (i.e. <50 vol.% crystals; Marsh, 1981; Yoshimura and Nakamura, 2011) at 100 MPa confining pressure can generate overpressures compatible with eruption (ΔP_{crit}; Jellinek and DePaolo, 2003; Rubin, 1995) when less than 0.025 wt.% of CO_2 has been flushed through the system at rates of $\geq 10^{-5}$ mol/m^2/s^{-1} (i.e. timescales to reach ΔP_{crit} shorter than about 10 years; Fig. 9). For lower CO_2-fluxes, viscous relaxation timescales of the surrounding crust are shorter than those required to reach ΔP_{crit}, hence volumetric expansion is accommodated entirely by viscous deformation of the crust (Fig. 9). For reservoirs located at 300 MPa, the minimum amount of injected CO_2 required to reach ΔP_{crit} is larger, increasing to ~0.06 wt.% for ΔP_{crit}=40MPa (Fig. 9). This is a direct consequence of the decreasing volume of a given mass of excess fluid phase with increasing depth of the reservoir. The minimum CO_2-flux required to trigger volcanic activity is essentially independent of the depth of the reservoir (Fig. 9). However,

considering that the viscosity of the crust likely decreases with increasing depth, higher CO_2-fluxes may be required to destabilise deeper reservoirs. If critical overpressures are not achieved, or the CO_2-flux is too low, progressive flushing simply increases excess fluid phase fraction and magma compressibility, thus enhancing the capacity of the reservoir to accommodate further magma input without eruption (Fig. 9). The increase of magma compressibility will also reduce our capacity of detecting volumetric variations within the magma reservoir by surface deformation measurements alone (Kilbride et al., 2016).

The progressive increase of excess fluid fraction and crystallinity associated with CO_2 flushing will lead eventually to the release of large quantities of H_2O-rich, and potentially mineralising, fluids from the magma body (Parmigiani et al., 2016; Fig. 8). As flushing continues, exsolved fluids become increasingly carbonic (Yoshimura and Nakamura, 2010), which could force the deposition of metals from metal-rich magmatic brines released in the initial phases of the CO_2 flushing event, when xH_2O of the released fluid is the highest (Blundy et al., 2015; Kokh et al., 2017; van Hinsberg et al., 2016). An alternative to this temporal evolution is that magma buoyancy becomes sufficiently large to destabilise the magma reservoir, before the magma has become too crystallised for an eruption to occur (Caricchi et al., 2014).

It is important to point out that overpressure calculations were performed assuming a closed system scenario (i.e. no progressive leakage of the excess volatile phase). This translates into the maximum possible volumetric expansion generated by CO_2 flushing, but also into the largest possible magma compressibility. Therefore, while leakage would decrease the volumetric expansion of the system, decreasing the overpressure with respect to the values provided here, leakage would also decrease magma compressibility and increase the resultant overpressure.

5. Conclusions

Volatile content and chemistry of melt inclusions from mafic and felsic systems suggest that CO_2 flushing is a widespread process affecting the chemical and physical evolution of magmas stored in the upper crust. Decompression-induced crystallisation, is also a viable mechanisms accounting for the variability observed in MIs, however our calculations show that trapping of a suite of melt inclusions recording the entire magma decompression path is unlikely (Figs. 4, 5).

Depending on the initial crystallinity of a CO_2-fluxed magma reservoir, sufficient overpressure resulting from the interaction between carbonic fluids and magma can either trigger a volcanic eruption or lead to the abrupt release of fluids. Because crystal content determines whether magmas can erupt (Marsh, 1981), initially crystal rich (40-50 wt.%) magmas attain their rheological locking point after only small amounts of injected CO_2, inhibiting their capacity to feed volcanic eruptions, but increasing the potential for excess fluid release (Parmigiani et al., 2016). The extraction of initially H_2O-rich fluids, that progressively become more carbonic, could provide an efficient mechanism for the extraction and precipitation of metals required for the formation of magmatic ore deposits (Kokh et al., 2017; van Hinsberg et al., 2016).

The interaction between CO_2 and magmas stored in the upper crust is an unavoidable consequence of the different solubility of H_2O and CO_2. CO_2 flushing exerts an important control on the chemical and physical evolution of magmatic systems that can be traced using both melt inclusions (Fig. 2) and detailed analysis of magmatic minerals (Blundy et al., 2015; Cashman and Blundy, 2013). We propose that CO_2 flushing is a previously unheralded process of destabilisation of magmatic systems,

capable of triggering both eruptions and impulsive release of potentially mineralising fluids.

REFERENCES

Barsanti, M., Papale, P., Barbato, D., Moretti, R., Boschi, E., Hauri, E., & Longo, A. (2009). Heterogeneous large total CO2 abundance in the shallow magmatic system of Kilauea volcano, Hawaii. Journal of Geophysical Research, 114(B12), 387–7. http://doi.org/10.1029/2008JB006187

Blythe, L. S., Deegan, F. M., Freda, C., Jolis, E. M., Masotta, M., Misiti, V., et al. (2015). CO_2 bubble generation and migration during magma–carbonate interaction. Contributions to Mineralogy and Petrology, 1–16. http://doi.org/10.1007/s00410-015-1137-4

Blundy, J, Cashman, K., 2008. Petrologic Reconstruction of Magmatic System Variables and Processes. Reviews in mineralogy and Geochemistry 69, 179–239. doi:10.2138/rmg.2008.69.6

Blundy, J, Cashman, K., 2001. Ascent-driven crystallisation of dacite magmas at Mount St Helens, 1980-1986. Contributions to Mineralogy and Petrology 140, 631–650.

Blundy, J., & Cashman, K. (2005). Rapid decompression-driven crystallization recorded by melt inclusions from Mount St. Helens volcano. Geology, *33*(10), 793. http://doi.org/10.1130/G21668.1

Blundy, J, Mavrogenes, J., Tattitch, B., Sparks, S., Gilmer, A., 2015. Generation of porphyry copper deposits by gas–brine reaction in volcanic arcs. Nature geoscience 8, 235–240. doi:10.1038/ngeo2351

Blundy, J, Cashman, K.V., Rust, A., Witham, F., 2010. A case for CO_2-rich arc magmas. Earth and Planetary Science Letters 290, 289–301. doi:10.1016/j.epsl.2009.12.013

Caricchi, L., Annen, C., Blundy, J., Simpson, G., Pinel, V., 2014. Frequency and magnitude of volcanic eruptions controlled by magma injection and buoyancy. Nature geoscience 7, 126–130. doi:10.1038/ngeo2041

Cashman, K., Blundy, Jon, 2013. Petrological cannibalism: the chemical and textural consequences of incremental magma body growth. Contributions to Mineralogy and Petrology 166, 703–729. doi:10.1007/s00410-013-0895-0

Cross, J.K., Tomlinson, E.L., Giordano, G., Smith, V.C., De Benedetti, A.A., Roberge, J., Manning, C.J., Wulf, S., Menzies, M.A., 2013. High level triggers for explosive mafic volcanism: Albano Maar, Italy. Lithos 190-191, 137–153. doi:10.1016/j.lithos.2013.11.001

Di Rocco, T., Freda, C., Gaeta, M., Mollo, S., & Dallai, L. (2012). Magma Chambers Emplaced in Carbonate Substrate: Petrogenesis of Skarn and Cumulate Rocks and Implications for CO_2 Degassing in Volcanic Areas. Journal of Petrology, 53(11), 2307–2332. http://doi.org/10.1093/petrology/egs051

Evans, B.W., Hildreth, W., Bachmann, O., Scaillet, B., 2016. In defense of magnetite-ilmenite thermometry in the Bishop Tuff and its implication for gradients in silicic magma reservoirs. Am Mineral 101, 469–482. doi:10.2138/am-2016-5367

Federico, C., Pietro Paolo Corso, Fiordilino, E., Cardellini, C., Chiodini, G., Parello, F., Pisciotta, A., 2010. degassing at La Solfatara volcano (Phlegrean Fields):

Processes affecting d. Geochim Cosmochim Ac 74, 3521–3538. doi:10.1016/j.gca.2010.03.010

Fowler, S. J., & Spera, F. J. (2008). Phase equilibria trigger for explosive volcanic eruptions. Geophysical Research Letters, 35(8), 1127–5. http://doi.org/10.1029/2008GL033665

Gaetani, G.A., O'Leary, J.A., Shimizu, N., Bucholz, C.E., Newville, M., 2012. Rapid reequilibration of H_2O and oxygen fugacity in olivine-hosted melt inclusions. Geol 40, 915–918. doi:10.1130/G32992.1

Ghiorso, M.S., Gualda, G.A.R., 2015. An H_2O-CO_2 mixed fluid saturation model compatible with rhyolite-MELTS. Contributions to Mineralogy and Petrology 1–30. doi:10.1007/s00410-015-1141-8

Gualda, G.A.R., Ghiorso, M.S., Lemons, R.V., Carley, T.L., 2012. Rhyolite-MELTS: a Modified Calibration of MELTS Optimized for Silica-rich, Fluid-bearing Magmatic Systems. Journal of petrology 53, 875–890. doi:10.1093/petrology/egr080

Iacono Marziano, G., Schmidt, B.C., Dolfi, D., 2007. Equilibrium and disequilibrium degassing of a phonolitic melt (Vesuvius AD 79 “white pumice”) simulated by decompression experiments. Journal of Volcanology and Geothermal Research 161, 151–164. doi:10.1016/j.jvolgeores.2006.12.001

Jellinek, A.M., DePaolo, D.J., 2003. A model for the origin of large silicic magma chambers: precursors of caldera-forming eruptions. Bulletin of Volcanology 65, 363–381. doi:10.1007/s00445-003-0277-y

Jolis, E.M., Freda, C., Troll, V.R., Deegan, F.M., Blythe, L.S., McLeod, C.L., Davidson, J.P., 2013. Experimental simulation of magma–carbonate interaction beneath Mt. Vesuvius, Italy. Contributions to Mineralogy and Petrology 166, 1335–1353. doi:10.1007/s00410-013-0931-0

Kilbride, B. M., Biggs, J., & Edmonds, M. (2016). Observing eruptions of gas-rich compressible magmas from space. Nature Communications, *7*, 1–8. http://doi.org/10.1038/ncomms13744

Kokh, M.A., Akinfiev, N.N., Pokrovski, G.S., Salvi, S., Guillaume, D., 2017. The role of carbon dioxide in the transport and fractionation of metals by geological fluids. Geochim Cosmochim Ac 197, 433–466. doi:10.1016/j.gca.2016.11.007

Marsh, B.D., 1981. On the Crystallinity, Probability of Occurrence, and Rheology of Lava and Magma. Contributions to Mineralogy and Petrology 78, 85–98.

Mason, E., Edmonds, M., Turchyn, A.V., 2017. Remobilization of crustal carbon may dominate volcanic arc emissions. Science 357. doi:10.1126/science.aan5049

Metrich, N., Allard, P., Spilliaert, N., Andronico, D., Burton, M., 2004. 2001 flank eruption of the alkali- and volatile-rich primitive basalt responsible for Mount Etna's evolution in the last three decades. Earth and Planetary Science Letters 228, 1–17. doi:10.1016/j.epsl.2004.09.036

Metrich, N., Bertagnini, A., Di Muro, A., 2010. Conditions of Magma Storage, Degassing and Ascent at Stromboli: New Insights into the Volcano Plumbing System with Inferences on the Eruptive Dynamics. Journal of petrology 51, 603–626. doi:10.1093/petrology/egp083

Moretti, R., Arienzo, I., Civetta, L., Orsi, G., & Papale, P. (2013). Multiple magma degassing sources at an explosive volcano. Earth and Planetary Science Letters, 367, 95–104. http://doi.org/10.1016/j.epsl.2013.02.013

Newman, S., Lowenstern, J.B., 2002. VOLATILECALC: a silicate melt-H_2O-CO_2 solution model written in Visual Basic for excel. Computers & Geosciences 28, 597–604.

Papale, P. (2005). Determination of total H_2O and CO_2 budgets in evolving magmas from melt inclusion data. Journal of Geophysical Research, 110(B3), B03208. http://doi.org/10.1029/2004JB003033

Papale, P., Moretti, R., Barbato, D., 2006. The compositional dependence of the saturation surface of H_2O+CO_2 fluids in silicate melts. Chemical Geology 229, 78–95.

Parmigiani, A., Faroughi, S., Huber, C., Bachmann, O., Su, Y., 2016. Bubble accumulation and its role in the evolution of magma reservoirs in the upper crust. Nature 532. doi:10.1038/nature17401

Pitzer, K.S., Sterner, S.M., 1994. Equations of state valid continuously from zero to extreme pressures for H_2O and CO_2. J. Chem. Phys. 101, 3111–3116. doi:10.1063/1.467624

Preece, K., Gertisser, R., Barclay, J., Berlo, K., Herd, R.A., Facility, E.I.M., 2014. Pre- and syn-eruptive degassing and crystallisation processes of the 2010 and 2006 eruptions of Merapi volcano, Indonesia. Contributions to Mineralogy and Petrology 168. doi:10.1007/s00410-014-1061-z

Riker, J.M., Blundy, J.D., Rust, A.C., Botcharnikov, R.E., Humphreys, M.C.S., 2015. Experimental phase equilibria of a Mount St. Helens rhyodacite: a framework for interpreting crystallization paths in degassing silicic magmas. Contributions to Mineralogy and Petrology 1–22. doi:10.1007/s00410-015-1160-5

Rubin, A.M., 1995. Getting Granite Dikes Out of the Source Region. J Geophys Res-Sol Ea 100, 5911–5929.

Sterner, S.M., Pitzer, K.S., 1994. An equation of state for carbon dioxide valid from zero to extreme pressures. Contributions to Mineralogy and Petrology 117, 362–374. doi:10.1007/BF00307271

Tramontano, S., Gualda, G. A. R., & Ghiorso, M. S. (2017). Internal triggering of volcanic eruptions: tracking overpressure regimes for giant magma bodies. Earth and Planetary Science Letters, 472, 142–151. doi: 10.1016/j.epsl.2017.05.014.

van Hinsberg, V.J., Berlo, K., Migdisov, A.A., Williams-Jones, A.E., 2016. CO2-fluxing collapses metal mobility in magmatic vapour. Geochemical Perspectives Letters 169–177. doi:10.7185/geochemlet.1617

Werner, C., Brantley, S., 2003. CO_2 emissions from the Yellowstone volcanic system. Geochemistry geophysics Geosystems 4, 387. doi:10.1029/2001JB000407

Yoshimura, S., Nakamura, M., 2011. Carbon dioxide transport in crustal magmatic systems. Earth and Planetary Science Letters 307, 470–478. doi:10.1016/j.epsl.2011.05.039

Yoshimura, S., Nakamura, M., 2010. Chemically driven growth and resorption of bubbles in a multivolatile magmatic system. Chemical Geology 276, 18–28. doi:10.1016/j.chemgeo.2010.05.010

Figure captions

Figure 1: Variation of dissolved H_2O and CO_2, crystal and fluid fraction as functions of H_2O dissolved in magma. Blue lines refer to calculations performed at 300 MPa, red at 100 MPa. a) coloured lines are H_2O and CO_2 solubility isobars for magma saturated in H_2O-CO_2 fluids with different molar fraction of H_2O (xH_2O); grey lines

are isopleths, indicating the H_2O and CO_2 dissolved in magma in equilibrium with fluids of fixed xH_2O. b) The continuous and dashed lines show, respectively, the evolution of the crystal (weight) and fluid (volume) fraction during CO_2 flushing as functions of dissolved H_2O.

Figure 2: Evolution of H_2O and CO_2 dissolved in melt undergoing CO_2 flushing as calculated by Rhyolite-MELTS (Gualda et al., 2012). All simulations started with magma saturated in H_2O. The diagrams are colour-contoured for wt.% of exsolved fluids (panel a), melt fraction (b), and temperature (c). Simulations were performed at fO_2 = NNO for a felsic magma with a composition equivalent to the average melt inclusion composition of the early phase of the Bishop Tuff eruption (Table 1; Gualda et al., 2012; Ghiorso and Gualda, 2015)

Figure 3: Evolution of H_2O and CO_2 dissolved in melt undergoing CO_2 flushing as calculated from Rhyolite-MELTS (Gualda et al., 2012). All simulations started with magma containing only H_2O (initially undersaturated). The diagrams are colour-contoured for wt.% of exsolved fluids (panel a), melt fraction (b), and temperature (c). The simulations were performed at fO_2 = NNO for a magma of basaltic composition (Metrich et al., 2004).

Figure 4: Evolution of H_2O and CO_2 dissolved in melt, and K_2O content of residual melt during CO_2 flushing calculated by Rhyolite-MELTS. Panels a and b are calculations performed for Bishop Tuff and c, d for Etna composition (see text and Table 1for more details). The colour contouring in panel a and c is for K_2O content of the residual melt. Colours in panels b and d are for the different confining pressures at which the simulations were performed.

Figure 5: Evolution of H_2O and CO_2 dissolved in melt , and K_2O content of residual melt during magma ascent. Panels a and b are calculations performed for Bishop Tuff

and c, d, e, and f are for Etna composition (see text and Table 1 for more details). The colour contouring in panels a, b and c is for K_2O content of the residual melt. Colour contouring in panels b, d and f indicates the evolution of the confining pressure during the simulations. The results shown in panels e and f were calculated starting with a fluid-saturated composition (Table 1). The arrowheads indicate the evolution of parameters during decompression.

Figure 6: Volatile and K_2O content of melt inclusions and recalculated excess equilibrium fluid fraction for melt inclusions from Mount St. Helens and Merapi volcanoes. a) Isobars (black lines) and isopleths (grey lines) are calculated using the model of Ghiorso and Gualda (2015) for rhyolitic magma with a composition equivalent to the average melt inclusion composition of the early phase of the Bishop Tuff eruption (Table 1; Gualda et al., 2012; Ghiorso and Gualda, 2015). Symbols are colour contoured for K_2O content. Inset shows the MI trajectories for the different processes affecting MIs; b) xH_2O of the excess fluid phase recalculated using the model of Ghiorso and Gualda (2015) assuming equilibrium and volatile saturation. Symbols are colour coded for calculated entrapment pressure increasing from blue to red. Inset shows the MI trajectories for the different processes affecting MIs; c) Same as panel a showing melt inclusions from Merapi. d) Same as panel b for melt inclusions from Merapi.

Figure 7: Volatiles, K_2O content of melt inclusions and recalculated fraction of excess fluids in equilibrium with melt inclusions from Etna and Stromboli volcanoes. a) Isobars (black lines) and isopleths (grey lines) are calculated using the model of Ghiorso and Gualda (2015) for basaltic (MORB) composition (Gualda et al., 2012). Symbols are colour contoured for K_2O content. b) xH_2O of the excess fluid phase recalculated using the model of Ghiorso and Gualda (2015) assuming equilibrium and

volatile saturation. Symbols are colour coded for calculated entrapment pressure increasing from blue to red. c) Same as panel a but for melt inclusions from Stromboli. d) Same as panel b but for melt inclusions from Stromboli.

Figure 8: Variations of melt weight fraction, excess fluid volume fraction, wt.% of exsolved H_2O and xH_2O of the excess fluid phase as functions of the wt.% of CO_2 injected into magma with different initial melt fractions. Black colour refers to melt fraction, green to excess fluid volume fraction, cyan to wt.% of exsolved H_2O, and red to xH_2O of the excess fluid phase. a, c) Contours of equal melt and bubble fractions as function of the wt.% of injected CO_2 at 100 and 300 MPa respectively. b) Section of panel a and c corresponding to the grey arrows showing evolution of melt and bubble fraction as functions of injected CO_2 (wt.%) for a magma with an initial melt fraction of 0.8. d, f) Contours of wt. % exsolved H_2O and xH_2O of excess fluid phase as functions of the wt.% of injected CO_2. e) Section of panel d and f corresponding to the grey arrows, showing the evolution of wt. % exsolved H_2O and xH_2O as functions of injected CO_2 (wt.%) for a magma with an initial melt fraction of 0.8.

Figure 9: Time required to inject CO_2 at different mass flux rates into a reservoir of 5000 km^3 volume and 1 km thickness. The red and blue areas provide the range of injected CO_2 required to reach an overpressure in the magma reservoir of 10 to 40 MPa for magma reservoirsd at a confining pressure of 100 and 300 MPa respectively. The brown area indicates the range of viscous relaxation timescales for an upper crust viscosity of 10^{19} and 10^{20} Pa s. The black lines represent the time required to inject a given amount of CO_2 for different mass fluxes. If the black lines intercept the red or blue regions prior to the brown region, the rate of CO_2 injection is sufficient to reach critical overpressures before viscous relaxation of the crust is achieved; white dashed lines indicate conditions compatible with volcanic eruption. Conversely, if the black

lines intercept the brown area, viscous relaxation of the crust occurs on shorter timescales than those required for overpressurisation of the magma reservoir to 10-40 MPa; green dashed lines indicate conditions favourable for magma accumulation and fluid release.

Figure S1: Evolution of H_2O and CO_2 dissolved in magma undergoing CO_2 flushing as calculated from rhyolite-MELTS (Gualda et al., 2012). The simulations all started from magma containing only water. The diagrams are colour-contoured for wt.% of exsolved fluids (panel a), melt fraction (b), and temperature (c). The simulations were performed considering a felsic magma of basaltic composition (Metrich et al., 2004). Calculations were performed at an oxygen fugacity fixed to a value equivalent to QFM.

Acknowledgments

L.C. and T.E.S. received funding from the European Research Council (ERC) under the European Union's Horizon 2020 research and innovation programme (grant agreement No. 677493 - FEVER). J.B acknowledges research funding from BHP. Detailed and insightful comments by Paolo Papale and an anonymous reviewer significantly improved this contribution.

Author Contributions

All authors contributed to the design of the study. L.C. and T.E.S. performed the calculations and drafted the first version of the manuscript. All authors contributed to the final version.

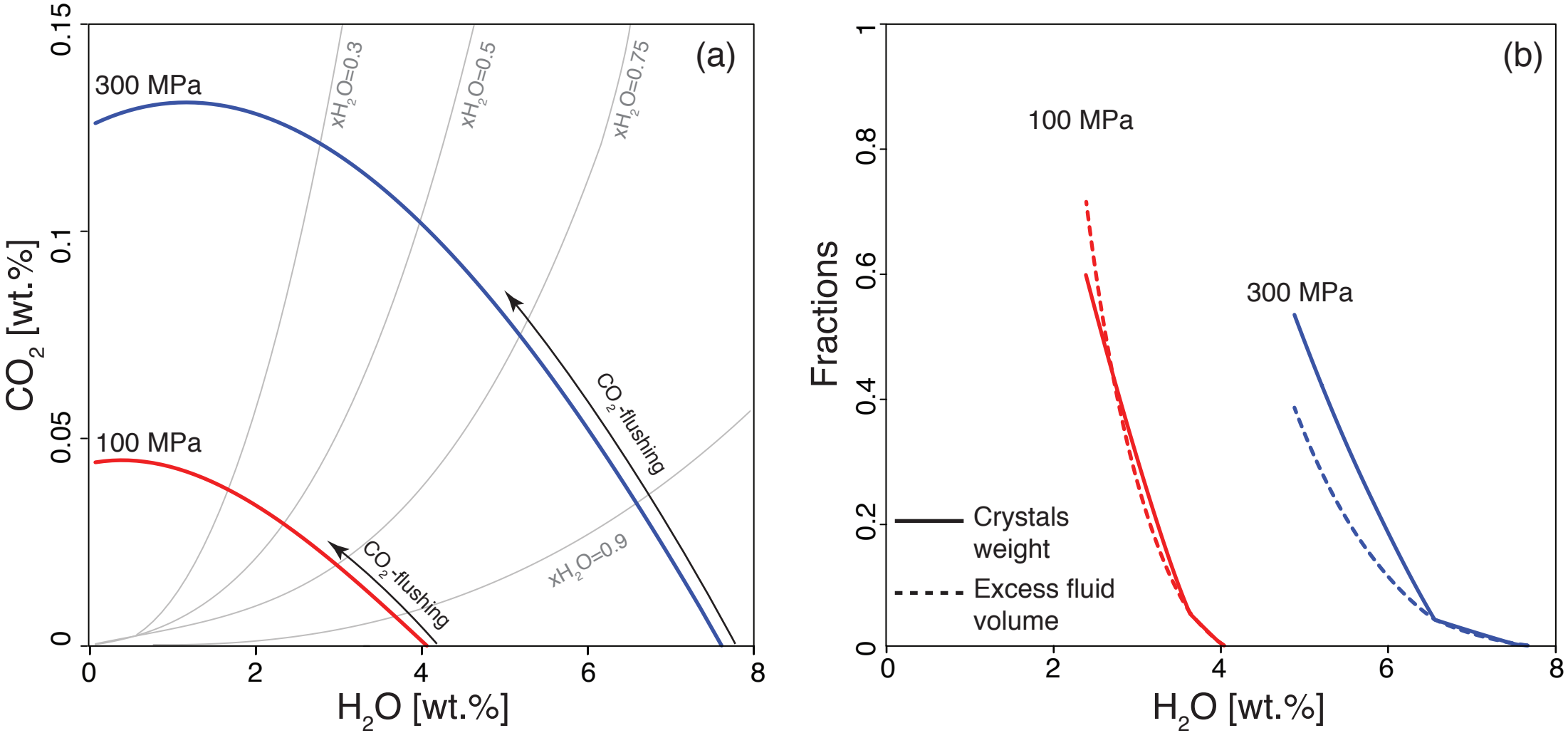
(a)
300 MPa
100 MPa
xH2O=0.3
xH2O=0.5
xH2O=0.75
xH2O=0.9
CO2-flushing
CO2-flushing
CO2 [wt.%]
H2O [wt.%]
0
0.05
0.1
0.15
0
2
4
6
8
(b)
100 MPa
300 MPa
Crystals weight
Excess fluid volume
Fractions
H2O [wt.%]
0
0.2
0.4
0.6
0.8
1
0
2
4
6
8

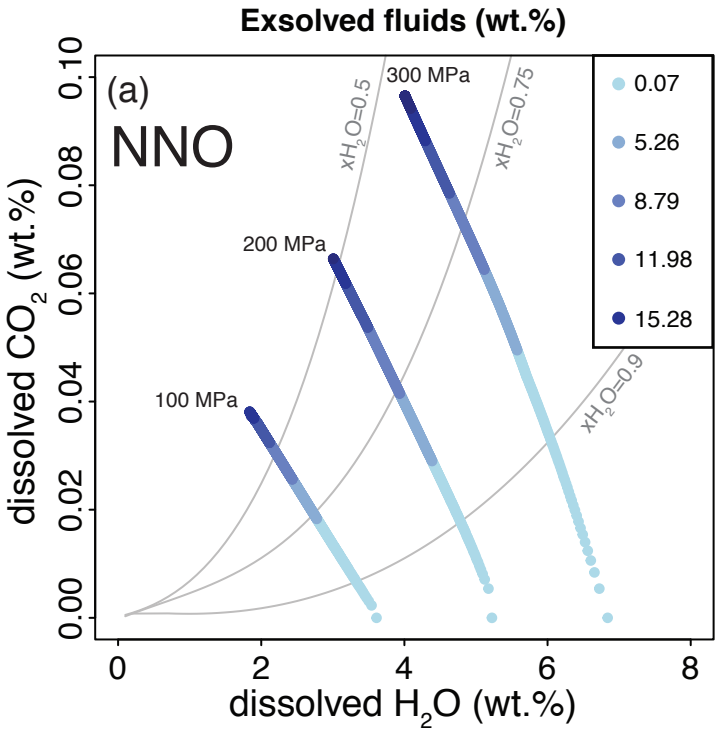
Exsolved fluids (wt.%)
(a)
NNO
300 MPa
200 MPa
100 MPa
xH2O=0.5
xH2O=0.75
xH2O=0.9
0.07
5.26
8.79
11.98
15.28
dissolved CO2 (wt.%)
dissolved H2O (wt.%)

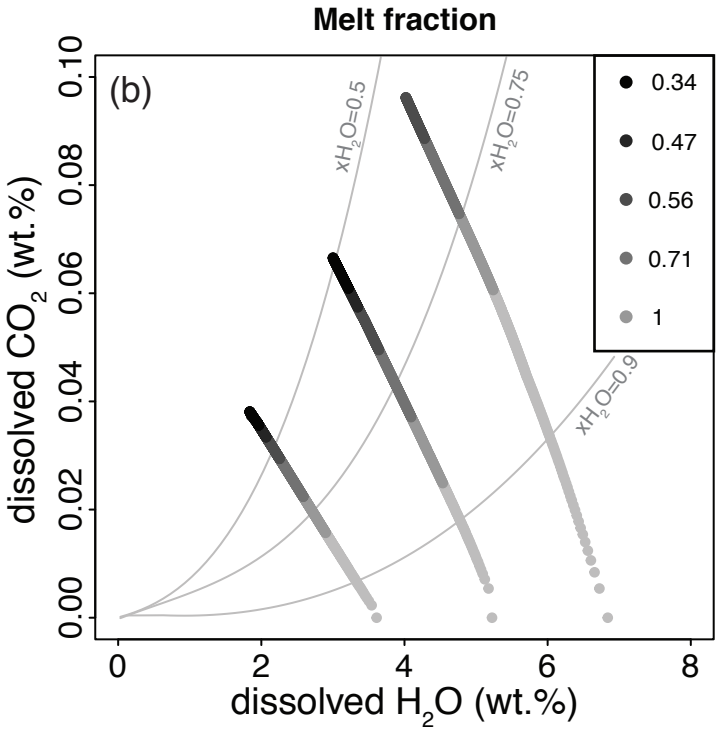
Melt fraction
(b)
xH2O=0.5
xH2O=0.75
xH2O=0.9
0.34
0.47
0.56
0.71
1
dissolved CO2 (wt.%)
dissolved H2O (wt.%)

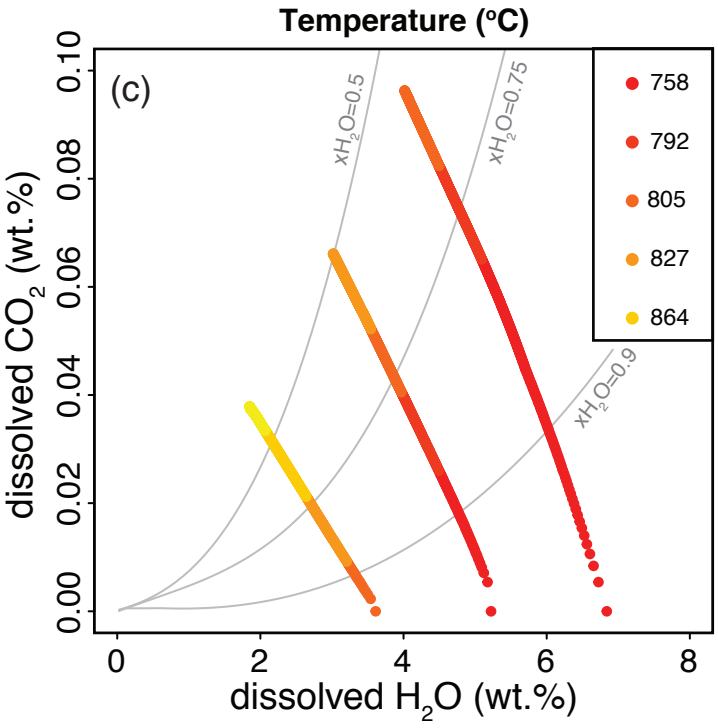
Temperature (°C)
(c)
xH2O=0.5
xH2O=0.75
xH2O=0.9
758
792
805
827
864
dissolved CO2 (wt.%)
dissolved H2O (wt.%)

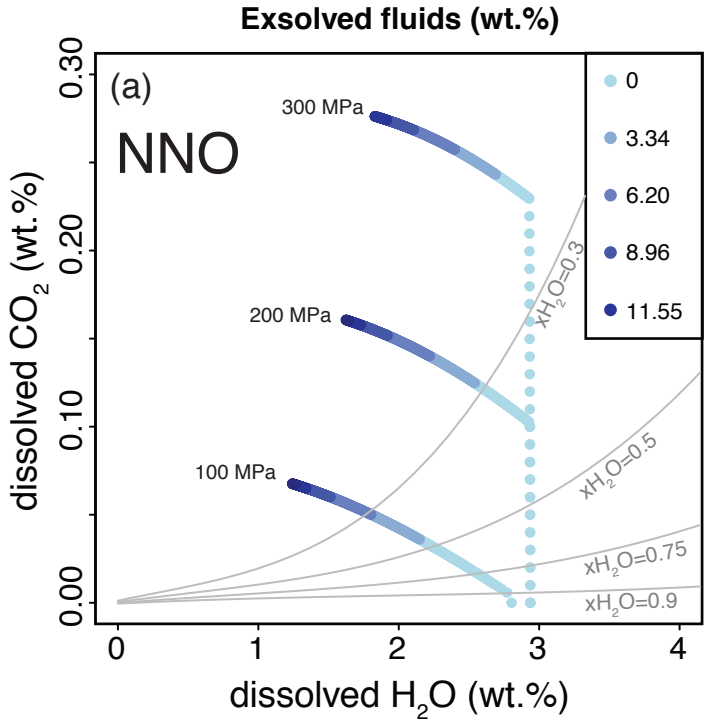
Exsolved fluids (wt.%)
(a)
NNO
300 MPa
200 MPa
100 MPa
0
3.34
6.20
8.96
11.55
xH2O=0.3
xH2O=0.5
xH2O=0.75
xH2O=0.9
dissolved CO2 (wt.%)
dissolved H2O (wt.%)
0.00
0.10
0.20
0.30
0
1
2
3
4

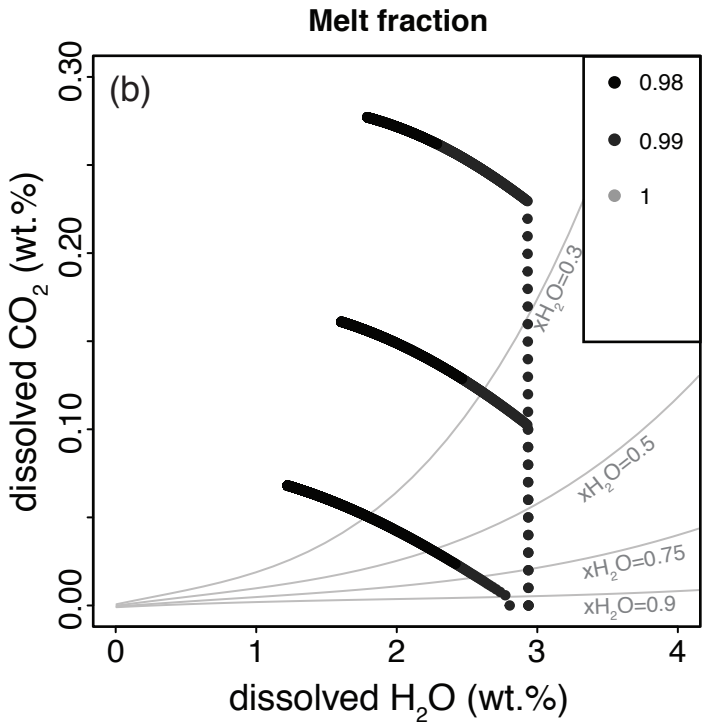
Melt fraction
(b)
0.98
0.99
1
xH2O=0.3
xH2O=0.5
xH2O=0.75
xH2O=0.9
dissolved CO2 (wt.%)
dissolved H2O (wt.%)
0.00
0.10
0.20
0.30
0
1
2
3
4

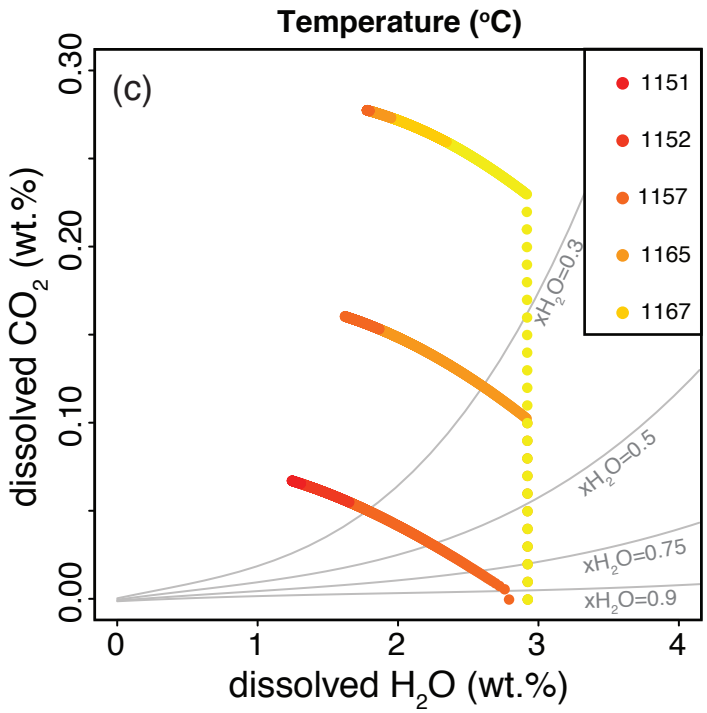
Temperature (°C)
(c)
1151
1152
1157
1165
1167
xH2O=0.3
xH2O=0.5
xH2O=0.75
xH2O=0.9
dissolved CO2 (wt.%)
dissolved H2O (wt.%)
0.00
0.10
0.20
0.30
0
1
2
3
4

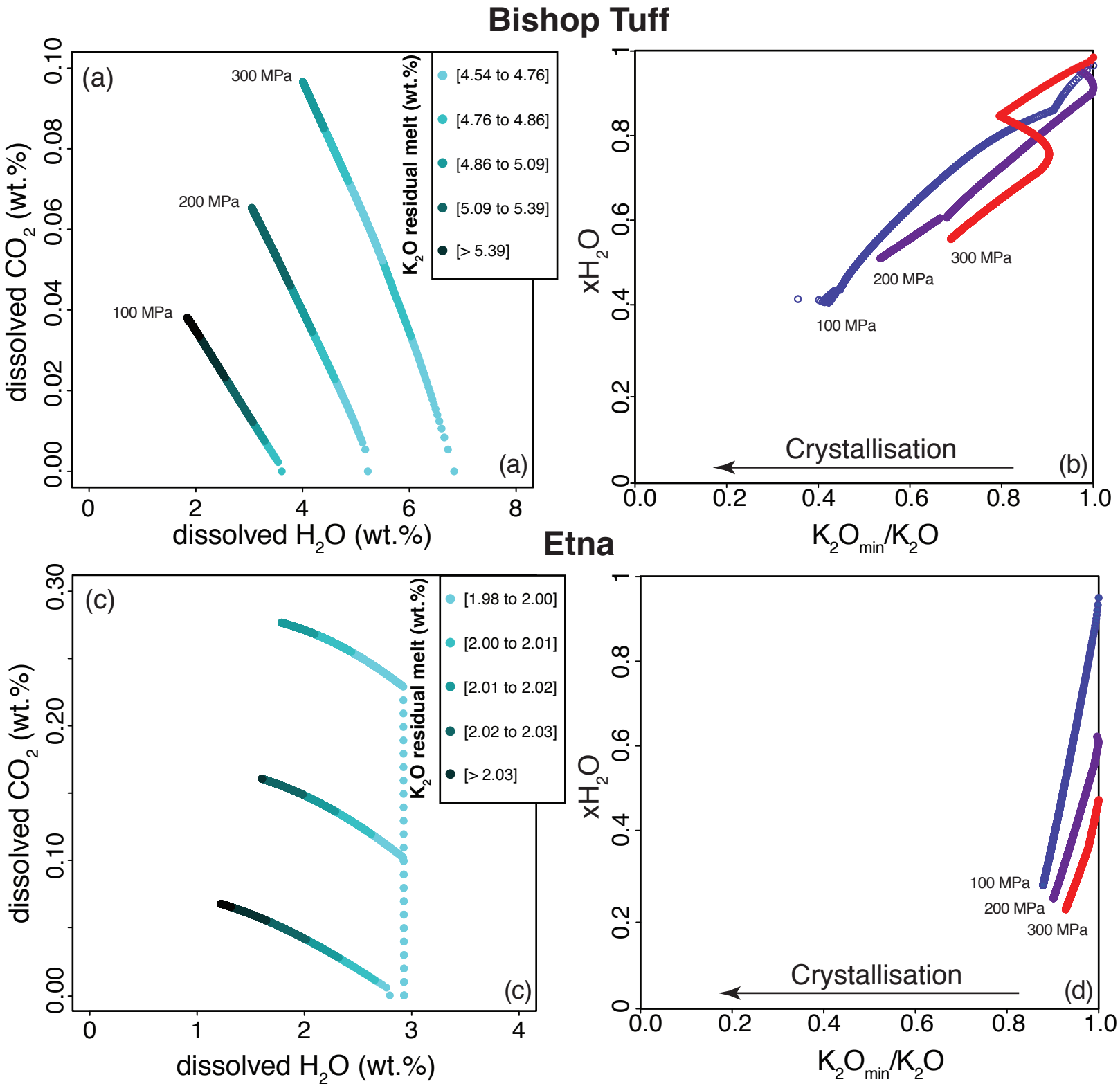
Bishop Tuff
(a)
300 MPa
200 MPa
100 MPa
K2O residual melt (wt.%)
[4.54 to 4.76]
[4.76 to 4.86]
[4.86 to 5.09]
[5.09 to 5.39]
[> 5.39]
dissolved CO2 (wt.%)
dissolved H2O (wt.%)
(b)
xH2O
K2Omin/K2O
Crystallisation
Etna
(c)
[1.98 to 2.00]
[2.00 to 2.01]
[2.01 to 2.02]
[2.02 to 2.03]
[> 2.03]
(d)

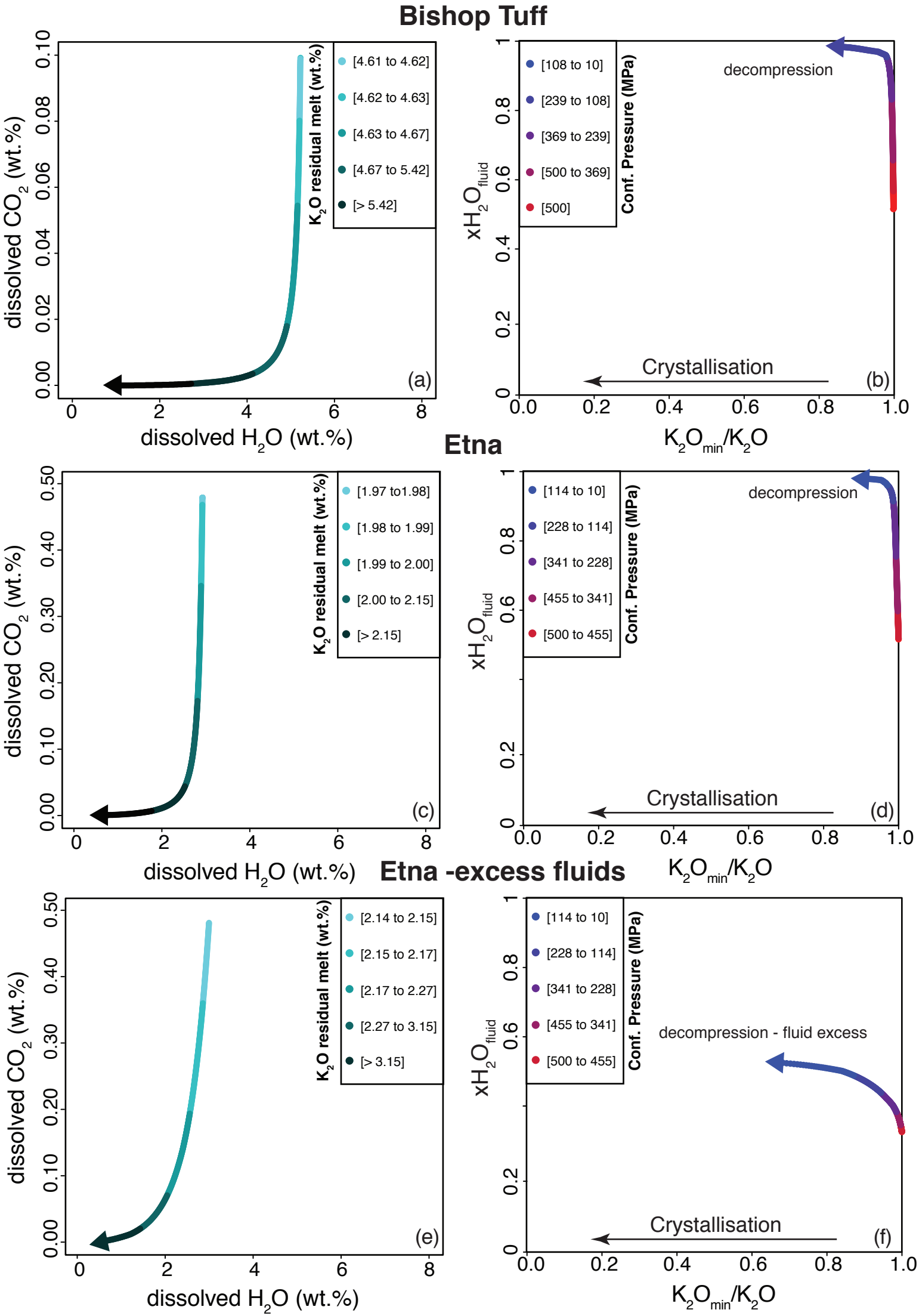
Bishop Tuff
dissolved CO_2 (wt.%)
dissolved H_2O (wt.%)
K_2O residual melt (wt.%)
[4.61 to 4.62]
[4.62 to 4.63]
[4.63 to 4.67]
[4.67 to 5.42]
[> 5.42]
(a)
xH_2O_{fluid}
K_2O_{min}/K_2O
Conf. Pressure (MPa)
[108 to 10]
[239 to 108]
[369 to 239]
[500 to 369]
[500]
decompression
Crystallisation
(b)
Etna
[1.97 to1.98]
[1.98 to 1.99]
[1.99 to 2.00]
[2.00 to 2.15]
[> 2.15]
(c)
[114 to 10]
[228 to 114]
[341 to 228]
[455 to 341]
[500 to 455]
(d)
Etna -excess fluids
[2.14 to 2.15]
[2.15 to 2.17]
[2.17 to 2.27]
[2.27 to 3.15]
[> 3.15]
(e)
decompression - fluid excess
(f)

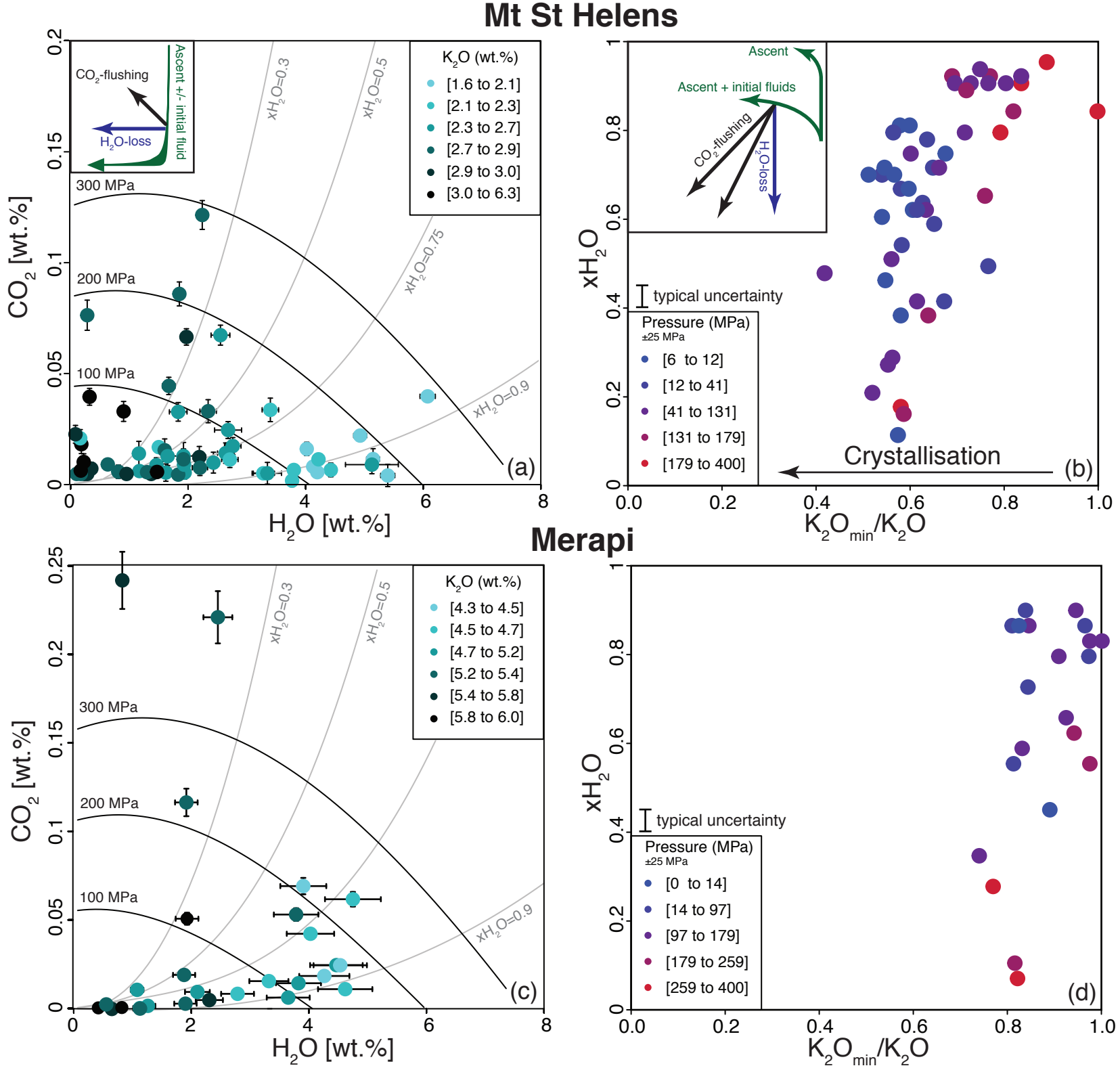
Mt St Helens
Merapi
CO2-flushing
H2O-loss
Ascent +/- initial fluid
Ascent
Ascent + initial fluids
K2O (wt.%)
[1.6 to 2.1]
[2.1 to 2.3]
[2.3 to 2.7]
[2.7 to 2.9]
[2.9 to 3.0]
[3.0 to 6.3]
[4.3 to 4.5]
[4.5 to 4.7]
[4.7 to 5.2]
[5.2 to 5.4]
[5.4 to 5.8]
[5.8 to 6.0]
300 MPa
200 MPa
100 MPa
xH2O=0.3
xH2O=0.5
xH2O=0.75
xH2O=0.9
CO2 [wt.%]
H2O [wt.%]
xH2O
K2Omin/K2O
typical uncertainty
Pressure (MPa)
±25 MPa
[6 to 12]
[12 to 41]
[41 to 131]
[131 to 179]
[179 to 400]
[0 to 14]
[14 to 97]
[97 to 179]
[179 to 259]
[259 to 400]
Crystallisation
(a)
(b)
(c)
(d)

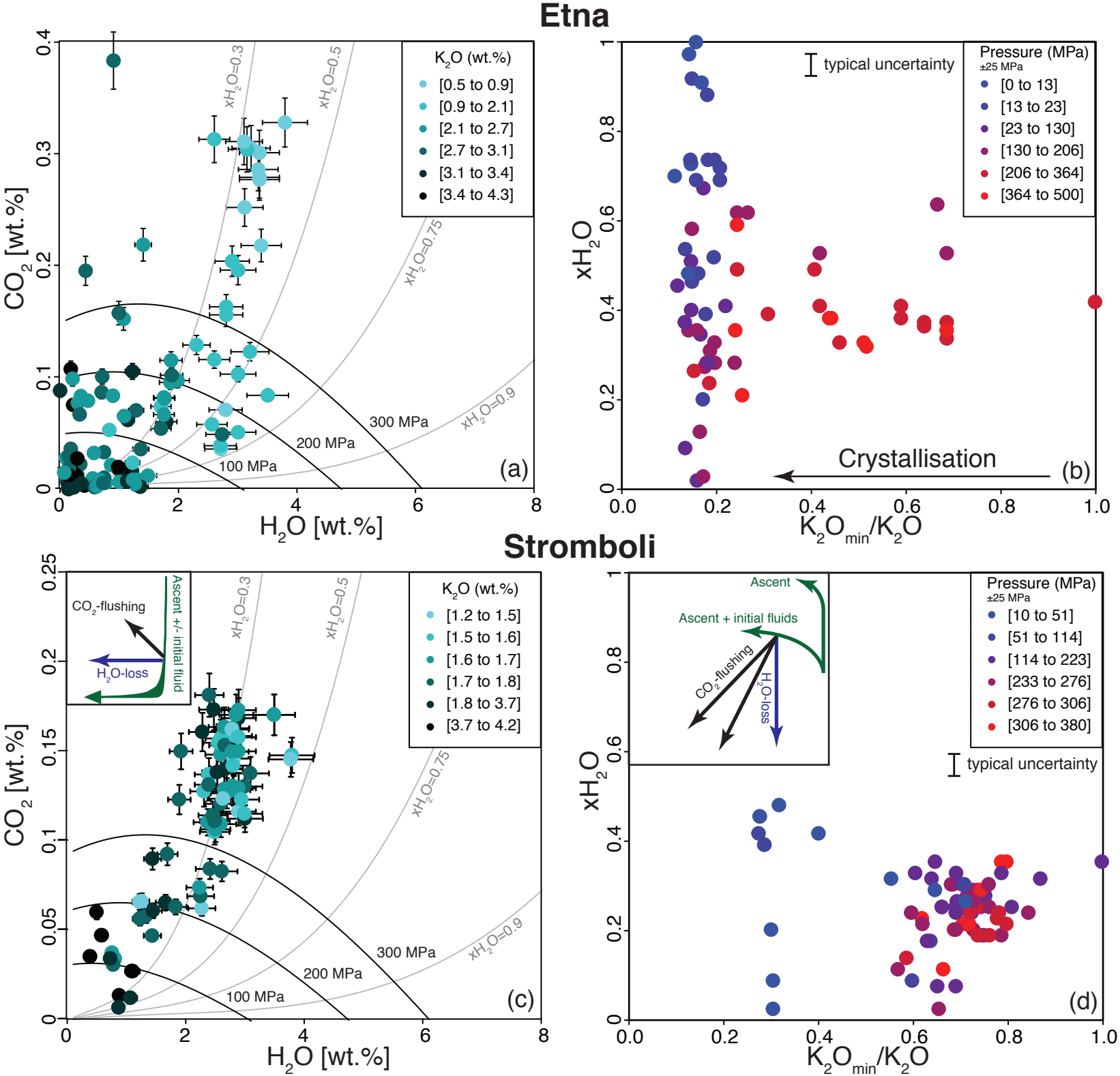
Etna
Stromboli
K2O (wt.%)
[0.5 to 0.9]
[0.9 to 2.1]
[2.1 to 2.7]
[2.7 to 3.1]
[3.1 to 3.4]
[3.4 to 4.3]
xH2O=0.3
xH2O=0.5
xH2O=0.75
xH2O=0.9
300 MPa
200 MPa
100 MPa
(a)
CO2 [wt.%]
H2O [wt.%]
typical uncertainty
Pressure (MPa)
±25 MPa
[0 to 13]
[13 to 23]
[23 to 130]
[130 to 206]
[206 to 364]
[364 to 500]
Crystallisation
(b)
xH2O
K2Omin/K2O
K2O (wt.%)
[1.2 to 1.5]
[1.5 to 1.6]
[1.6 to 1.7]
[1.7 to 1.8]
[1.8 to 3.7]
[3.7 to 4.2]
CO2-flushing
H2O-loss
Ascent +/- initial fluid
(c)
Ascent
Ascent + initial fluids
CO2-flushing
H2O-loss
Pressure (MPa)
±25 MPa
[10 to 51]
[51 to 114]
[114 to 223]
[233 to 276]
[276 to 306]
[306 to 380]
typical uncertainty
(d)

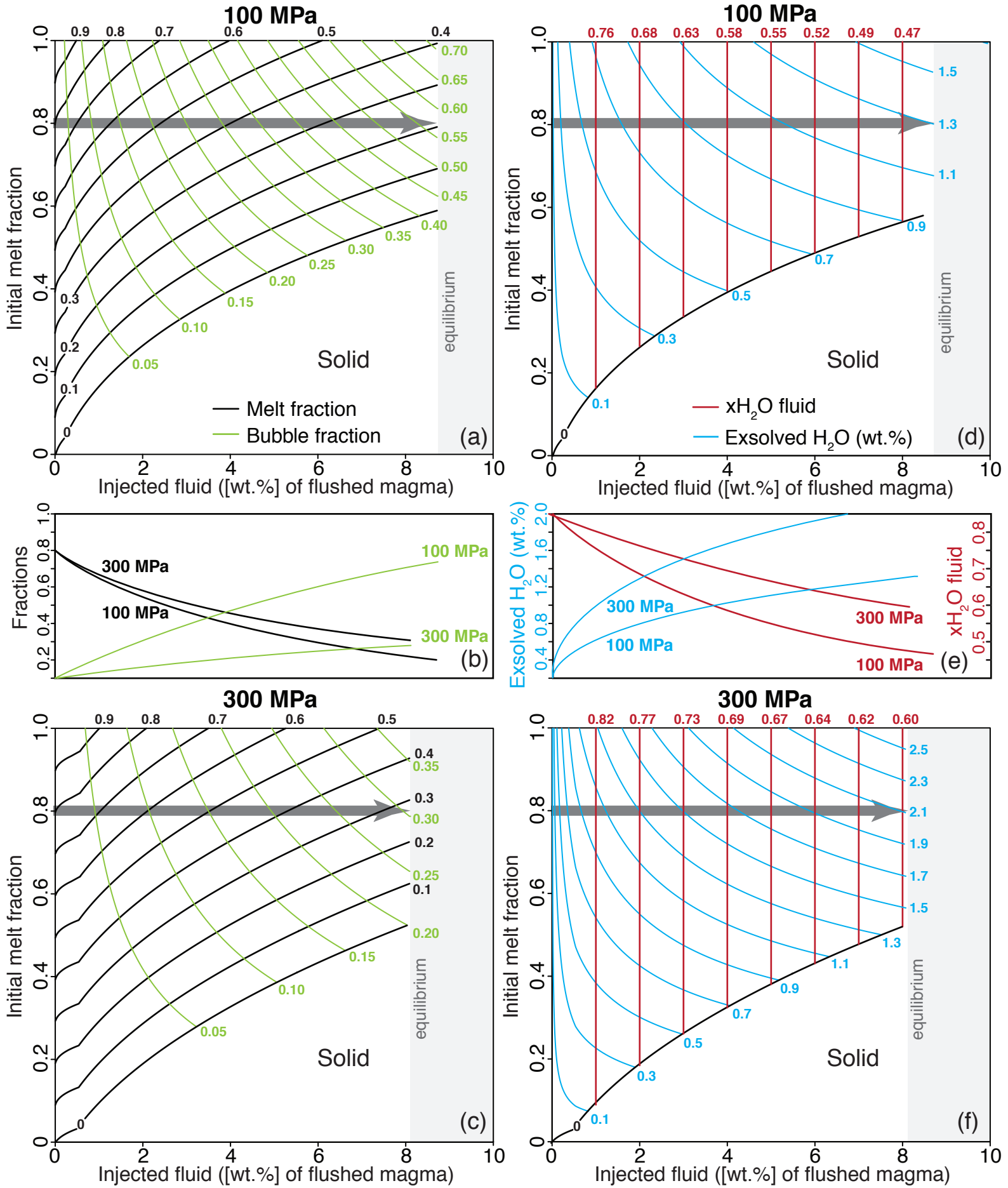
100 MPa
Initial melt fraction
Injected fluid ([wt.%] of flushed magma)
Solid
equilibrium
Melt fraction
Bubble fraction
(a)
xH2O fluid
Exsolved H2O (wt.%)
(d)
Fractions
300 MPa
100 MPa
(b)
Exsolved H2O (wt.%)
xH2O fluid
(e)
(c)
(f)

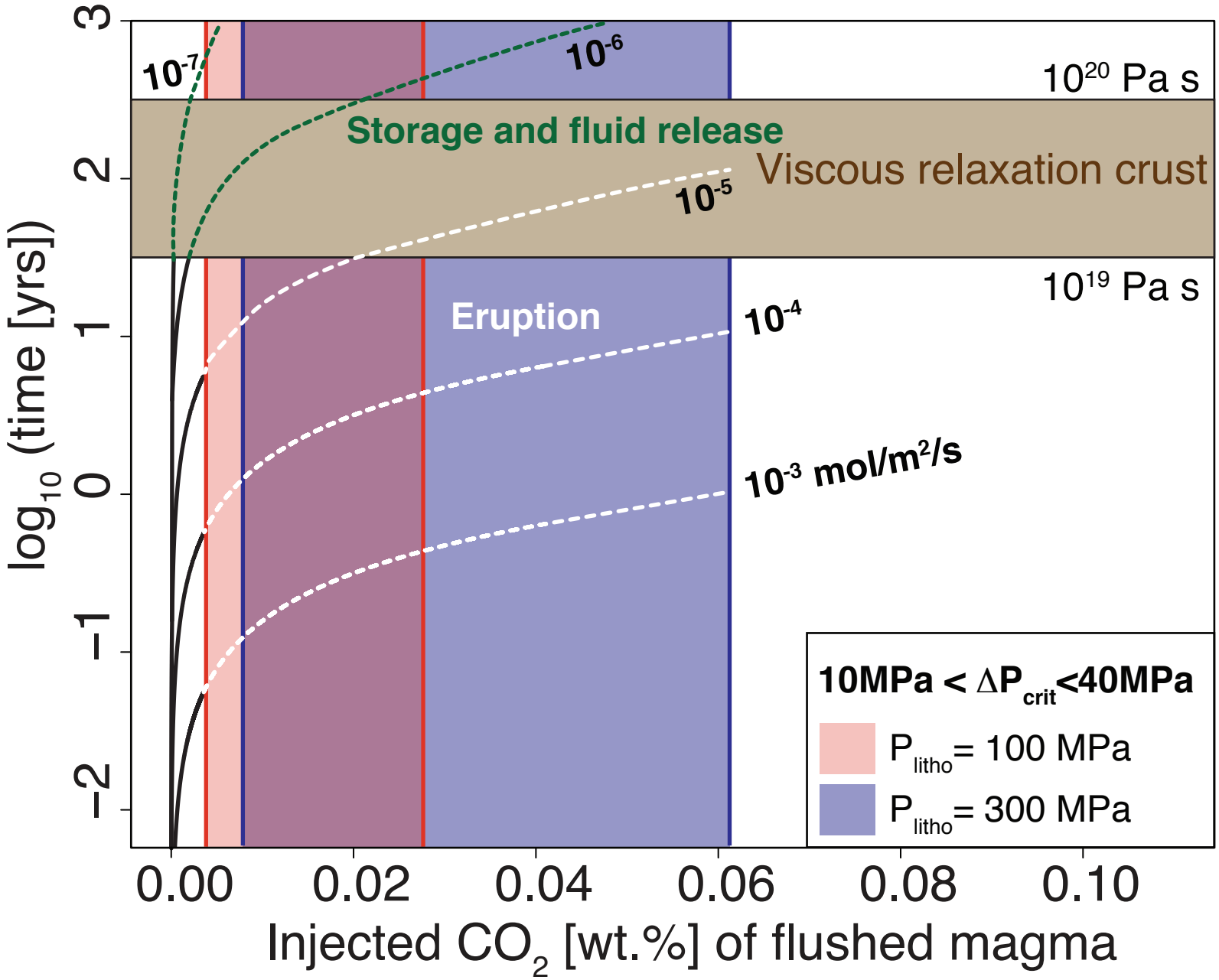
3
2
1
0
−1
−2
log10 (time [yrs])
0.00
0.02
0.04
0.06
0.08
0.10
Injected CO2 [wt.%] of flushed magma
10-7
10-6
10-5
10-4
10-3 mol/m2/s
10^20 Pa s
10^19 Pa s
Storage and fluid release
Viscous relaxation crust
Eruption
10MPa < ΔPcrit<40MPa
Plitho= 100 MPa
Plitho= 300 MPa

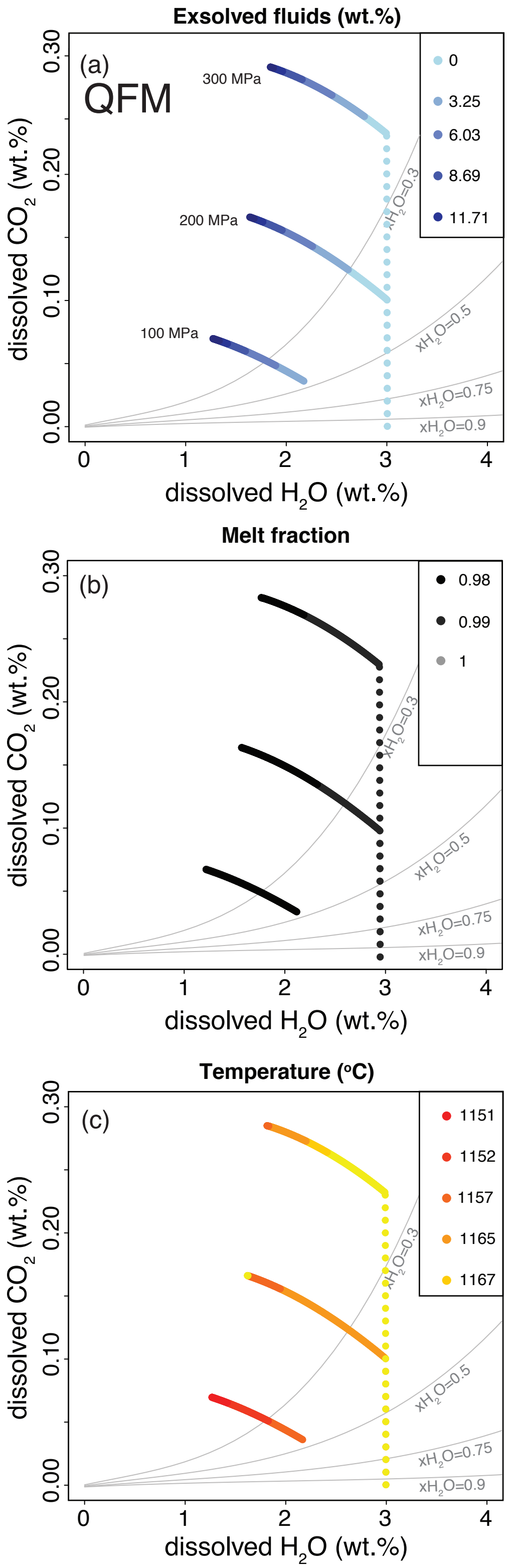
Exsolved fluids (wt.%)
(a)
QFM
300 MPa
200 MPa
100 MPa
0
3.25
6.03
8.69
11.71
xH2O=0.3
xH2O=0.5
xH2O=0.75
xH2O=0.9
dissolved CO2 (wt.%)
dissolved H2O (wt.%)
Melt fraction
(b)
0.98
0.99
1
Temperature (°C)
(c)
1151
1152
1157
1165
1167